ORIGINAL PAPER

Secondary toppling failure analysis and optimal support design for ignimbrites in the Ihlara Valley (Cappadocia, Turkey) by finite element method (FEM)

Mehmet Sari

Abstract Kizilkaya ignimbrite, characterized by a blocky structure in the Ihlara Valley (Cappadocia, Turkey), poses many hazards to visitors and the human-made churches and dwellings carved in the valley slopes. The instability mechanism in the valley should be carefully investigated to determine and implement a suitable prevention method. For this purpose, the finite element method (FEM) models were developed in RS2 software to illustrate the problem of progressive failure in the valley's cliffs. A simple geometry represented the rock strata and its surroundings. The effect of columnar structure on the cliff stability was mimicked as a jointed medium in two-dimensional numerical models. The results of FEM models revealed that as the stage of failure progresses in the slope, the strength reduction factor decreased subsequently from 2.05 to 0.45. These models correctly captured the prevailing failure mechanisms observed in the valley slopes. Depending on the size of the rock blocks described in the FEM analysis, an effective support system was proposed to remedy the slope failure. It was found that fully bonded rock bolts with a length of at least 2.5 times the width of a typical block should be implemented with a certain grid pattern. The study clearly showed that it was promising to realize a numerical solution to secondary toppling failure in a jointed rock mass using the FEM.

1 Introduction

Ihlara Valley, located approximately 35 km southeast of Aksaray city, is one of the most popular sites for tourists visiting the Cappadocia region in Turkey due to its richness in natural beauty, historical and cultural heritage (Fig. 1a). The 14 km long deep and narrow canyon was shaped both by the progressive failure of rock slopes due to water and wind erosion and the incision of bedrocks by the drainage system (Doğan et al. 2019). Due to its unique landscape, which includes 105 rock-hewn churches with frescos and around five thousand dwellings dating back to the early Byzantine era (ninth century), the canyon attracts around half a million local and foreign visitors every year (Varnacı-Uzun and Somuncu 2015). The site is recorded as a natural and historical heritage area protected by legislation (Official Gazette 1990); however, structurally controlled failures, especially toppling failures in the above hard ignimbrite rock, cause many hazards to visitors and the human-made

M. Sari (✉)
Department of Mining Engineering, Aksaray University, 68100 Aksaray, Turkey
e-mail: mehmetsari@aksaray.edu.tr

Fig. 1 **a** View of the Ihlara Valley from the main entry, **b** One of the fallen blocks in the valley, **c** Columnar structure of the Kizilkaya ignimbrite

structures (caves, dwellings, churches, and settlements) carved in the below soft tuffs. Large-sized rock blocks fallen from the columnar structure can sometimes block access to these buildings or even result in complete damage over time (Fig. 1b, c). Artificial caves and churches at the cliff's base further promote instability in the Ihlara Valley. The stability of these rock structures should be carefully investigated, and proper remedial measures should be implemented to protect the visitors from rock falls during their stay and preserve the natural and historical heritage in the long term.

The rock slope stability depends on the frequency, orientation, and shear strength properties of fractures presenting in the rock mass. These properties also determine the potential mode of failures, namely rotational, planar and wedge slides, and toppling failure (Hoek and Bray 1991). Kinematical, analytical, and numerical methods developed in the previous years have facilitated quick and accurate results to analyze circular, planar, and wedge failure modes in slope design practice (Sari 2019). Toppling is considered as one of the most complex failure mechanisms in the engineering geology field (Evans 1981; Zanbak 1983; Aydan and Kawamato 1992; Adhikary et al.

1997; Alejano and Alonso 2005; Tatone and Grasselli 2010; Amini et al. 2017). However, compared to the sliding mode of failure, only a limited amount of research has been undertaken concerning this type of failure. Since examples of different types of toppling failures have been identified in many locations worldwide, toppling is an important failure type that requires additional research into slope stability. Although some other classifications have been proposed for the toppling failures (Cruden 1989), a widely accepted one by the engineering geology community is suggested by Goodman and Bray (1976), who categorized toppling failures primary and secondary based on field observations. In primary toppling failures (flexural, blocky, and block-flexure), the rock mass weight is the principal factor causing instability, whereas, in secondary toppling with five subtypes, other natural or human-made external factors cause the failure.

As shown in Table 1, many researchers worked on the primary classification system, including block, flexural, and the block-flexural toppling of various cases. A limited number of studies were conducted using numerical modeling for the secondary toppling failure analysis, especially for toppling and slumping subtype. Evans (1981) conducted the most comprehensive study on the secondary toppling failure analysis. He used a stress redistribution method to analytically analyze the six possible failure mechanisms during secondary toppling failure. He concluded that bearing capacity failure, differential settlement due to weathering, and creep with associated stress redistribution were the most likely failure mechanisms. Amini et al. (2017) studied the slide-toe toppling failure mechanism by several tests conducted on physical models under a static condition with a new tilting table apparatus. The authors proposed a theoretical approach based on limit equilibrium analysis and developed alternative expressions for the stability analysis of this type of failure. Spreafico et al. (2017) attempted to resolve the mechanisms driving the development of secondary toppling at rocky hill boundaries in the San Leo area in Italy. They investigated the effect of the softening of basal clay shales and erosion due to seepage on the cliff failure using finite element method (FEM) models. They showed that using the Voronoi fracture simulation approach within continuum codes was promising in simulating intact rock failure within rock slopes.

Amini et al. (2018) described the mechanism of slide-head toppling failure with physical models and theoretical formulation. They found acceptable agreements between the analytical and experimental results. Amini and Aredestani (2019) studied a slide-toe toppling failure observed in an open-pit mine in Iran. They modified an existing analytical solution developed for the analysis of static slide-toe toppling failure. The comparison between the analytical, numerical, and field results showed satisfactory agreement. Sarfaraz et al. (2019) conducted a numerical analysis of slide-head toppling failure. They found good agreement between the numerical modeling results and the pre-existing physical modeling and the analytical method proposed by Amini et al. (2018). Sarfaraz and Amini (2020b) examined slide-toe toppling through a series of numerical modeling. They concluded that DEM numerical code was well capable of analyzing this type of toppling failure. A recent study by Haghgouei et al. (2020) proposed an analytical solution for toppling and slumping failure in rock slopes. Their study showed that the toppling and slumping failure could be observed if rock columns exert pressure on the underlying continuous weak rock or soil mass, which leads to a differential settlement at the base of each rock column or a circular shear failure in the continuous basal mass. As a result, an asymmetrical stress distribution under rock columns near the slope crest could be observed. The non-equality of stress on both sides of a column causes a non-uniform settlement and, consequently, leads to a toppling failure known as toppling-slumping.

The purpose of this paper is to study the mechanism of instabilities that occurred in the Kizilkaya ignimbrite characterized by a blocky structure in the cliffs of the Ihlara Valley using numerical methods. The slopes in the valley are mostly subject to the fourth subtype of secondary toppling failure according to Goodman and Bray's (1976) classification, which is toppling and slumping failure induced by differential settlement and shear failure due to basal weathering. Three separate FEM scenarios were examined using RS2 (Rocscience Inc. 2019a) software to capture the stages of this particular failure phenomena accurately. According to the numerical analysis findings, a support system with optimum design parameters was then proposed to stabilize the valley's block failures.

Table 1 Summary of toppling failure types and analysis methods studied in the literature

Study	Failure type				Analysis method			
	BT	FT	BF	ST	AN	EX	NU	PR
Evans (1981)				✔	✔			
Zanbak (1983)	✔				✔			
Scavia et al. (1990)	✔							✔
Aydan and Kawamoto (1992)		✔				✔		
Barla et al. (1995)	✔					✔	✔	
Adhikary et al. (1997)		✔				✔		
Lanaro et al. (1997)	✔					✔	✔	
Sagaseta et al. (2001)	✔				✔			
Nichol et al. (2002)	✔	✔					✔	
Muralha (2003)	✔						✔	✔
Alejona and Alanso (2005)	✔	✔					✔	
Amini et al. (2009)		✔			✔			
Brideau and Stead (2010)	✔						✔	
Alejano et al. (2010)			✔		✔		✔	
Tatone and Grasselli (2010)	✔							✔
Liu et al. (2010)	✔				✔			
Majdi and Amini (2011)		✔			✔			
Amini et al. (2012)			✔		✔			
Mohtarami et al. (2014)			✔		✔		✔	
Babiker et al. (2014)	✔				✔			
Smith (2015)	✔	✔			✔			
Alejano et al. (2015)	✔				✔	✔		
Amini et al. (2017)				✔	✔	✔		
Spreafico et al. (2017)				✔			✔	
Amini et al. (2018)				✔	✔	✔		
Zhang et al. (2018)		✔			✔			
Sun et al. (2018)	✔				✔		✔	
Bowa et al. (2018)	✔				✔			
Roy and Maheshwari (2018)	✔							✔
Amini and Ardestani (2019)				✔	✔		✔	
Zheng et al. (2019)			✔		✔		✔	
Sarfaraz et al. (2019)				✔			✔	
Sarfaraz (2020)		✔			✔			
Sarfaraz and Amini (2020a)			✔				✔	
Sarfaraz and Amini (2020b)				✔			✔	
Azarafza et al. (2020)	✔	✔	✔		✔		✔	
Haghgouei et al. (2020)				✔	✔			

2 Study Area

2.1 The Geological Setting

The Ihlara Valley, about 14 km in length and covering 52 km², is located near Aksaray city in a protected area (Ihlara Special Protection Area, ISPA). ISPA, having an average altitude of 1300 m above sea level, contains a vast amount of natural and cultural values of geological, archaeological, morphologic, biological, agricultural, and tourism. Due to joint systems developed on different lithological units, especially in the

Kizilkaya ignimbrite, interesting rock shapes and geomorphologic landscapes have been formed along the valley by water and wind erosion. Every day, thousands of tourists visit the rock-cut churches and dwellings excavated into the valley's cliffs. The valley lies in a complex tectonic environment within the talc-alkaline Central Anatolian volcanic province, which is bordered by two large Quaternary central stratovolcanoes: Mt. Erciyes (3917 m) on the eastern margin and Mt. Hasandagi (3257 m) on the southwestern margin of the Cappadocia region (Fig. 2a).

The stratigraphy of ISPA is mainly composed of Tertiary-Quaternary volcanic units, including the pyroclastic rocks of Hasandagi ashes, Selime tuff, Kizilkaya ignimbrite (Fig. 2b). Doğan et al. (2019) recently hypothesized that the uppermost geologic formation giving the region's topography, the Hasandagi ashes, originated from Mt. Hasandagi as debris avalanche. It displays an extensive distribution nearby the Ihlara Valley and consists mostly of volcanic ash and lapilli size pumice fragments. Its thickness varies in the study area from 10 to 120 m. The Kizilkaya
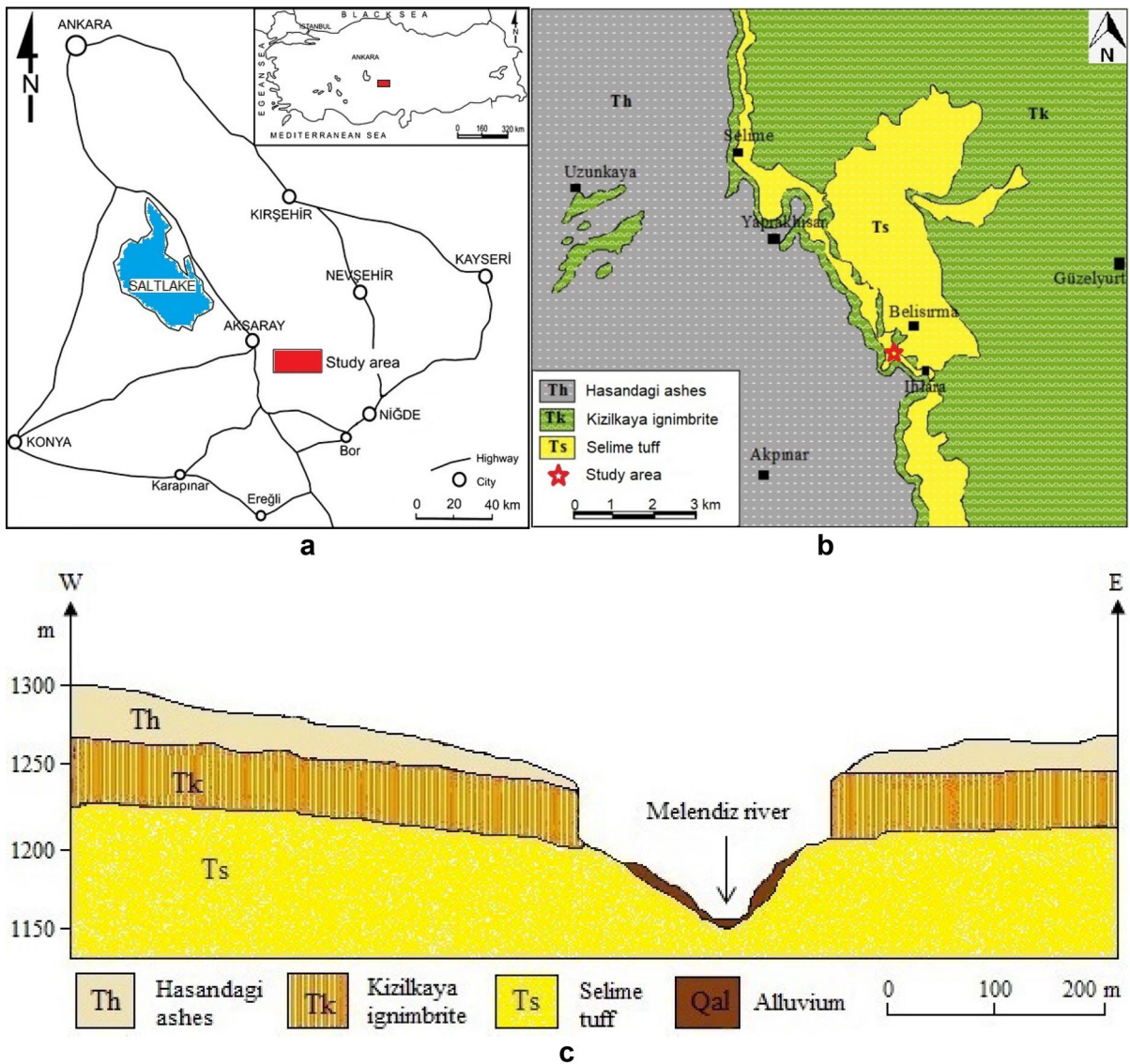
Fig. 2 a Location map of the study area, b Geologic map of the study area, c A simple representative E-W cross-section of the Ihlara Valley

(means "red rock" in Turkish) ignimbrite mainly comprises distinct flow units, typically welded with well-built columnar jointing, forming prominent cliffs and precipitous canyon walls. The columnar jointing in the rock unit might have developed due to tensional fracturing induced by thermal stresses during rock massif cooling. This joint system is a common feature of the volcanic rocks frequently observed in the Cappodocia region (Topal and Doyuran 1997; Ulusay et al. 2006). Kizilkaya ignimbrite's age is dated to 5.19 ± 0.07 Ma by the Ar–Ar method (Aydar et al. 2012). Le Pennec et al. (1994) indicated that the Kizilkaya ignimbrite covers an area greater than 10,600 km^2, thus being the most widespread unit in the Cappadocia region and has a volume of 180 km^3. In the valley, its thickness ranges between 4 and 60 m with an average of 25 m. The Kizilkaya ignimbrite is underlain by soft Selime tuff (named after Beekman 1966), which is bright beige and highly prone to erosion. This unit forms the base of the valley, and many "fairy chimneys", a surreal landscape of carved-out towering rock formations with caps characteristic to Cappadocia region, were observed near Selime village in this unit due to its unwelded nature (Yilmaz et al. 2012). A cooking zone (or air-fall ash layer) with a maximum height of 20 cm between Selime tuff and Kizilkaya ignimbrite can also be observed along the valley. The youngest unit in the area is the Quaternary aged river terraces and fluvial sediments deposited along the Melendiz River and its tributaries (Fig. 2c).

2.2 Failure Mechanism in the Valley

Many geological and geotechnical factors can contribute to the fourth subtype secondary toppling failures in nature. The frequency and persistence of fracturing and the amount of undercutting (i.e., erosion) and basal weathering govern the extent of the rock masses subjected to the instability problem (Spreafico et al. 2017). Erosion caused by various agents such as wind and water has an extreme effect on the formation of "fairy chimneys" and the stability of natural slopes of valleys in the Cappadocia region (Kaşmer et al. 2013). The erosion becomes important at the toe of steep valley slopes resulting in loss of support and causing slope failures when it reaches a certain amount. In the Ihlara Valley, weathering-related slope failures are a long process in terms of geological time. The weathering (erosion) rate of

rocks forming the valley slopes was determined based on both field and laboratory measurements (Ergüler 2009, Yilmaz et al. 2012). Ergüler (2009) found that the weathering rate changed between 0.4 and 2.5 mm/year for the softer part of Kavak members (the Selime tuff counterpart in this study). Yilmaz et al. (2012) stated that the Kizilkaya ignimbrite forming the cap rock was less affected by the weathering and hydrothermal processes because of its welded structure and high silica content. They calculated an annual erosion rate of 1.2 mm in the Selime tuff, and the rainfall was the most important agent in this process. Although the fundamental geological and geomorphological features of weathering-related slope failures have been recognized concerning both soil-like and rock-like materials, little attention has been given to the mechanics and kinematics of the most important instability types for weathered materials (Calcaterra and Parise 2010).

A simple schematic illustration of the secondary toppling failure mechanism in the valley slopes is reproduced in Fig. 3. It is proposed as a conceptual model to analyze the failure process in the valley. Basically, it comprises four subsequent stages. The first stage represents the rock structure's original geological condition in the valley cliffs (Fig. 3a). The influence of a changing climatic and meteorological condition is represented in the second stage (Fig. 3b). In this stage, runoff surface water infiltrates into the underlying Selime tuff through sub-vertical orthogonal joints developed during the rapid cooling of Kızılkaya ignimbrite deposits. Since the joints are mostly persistent, excess surface water can be easily drained down in the slope crest. The soft Selime tuff underneath is more vulnerable to deterioration from multiple cycles of wetting–drying and freezing–thawing processes (Binal 1996). It can be more deeply weathered and disintegrated by the associated weathering processes effective in the region. In the third stage, the toe of the slope subsequently erodes, and the weathered tuff zone underneath consequently losses its bearing capacity to carry overlaying rigid blocks separated by the vertical joints. At this stage, a measure of differential settlement at the base of each rock column due to non-equal stress redistribution after basal weathering, a concept postulated by Evans (1981) and Haghgouei et al. (2020), may also occur (Fig. 3c). In the last stage, the toppling and slumping failure occur due to sliding the detached block over the
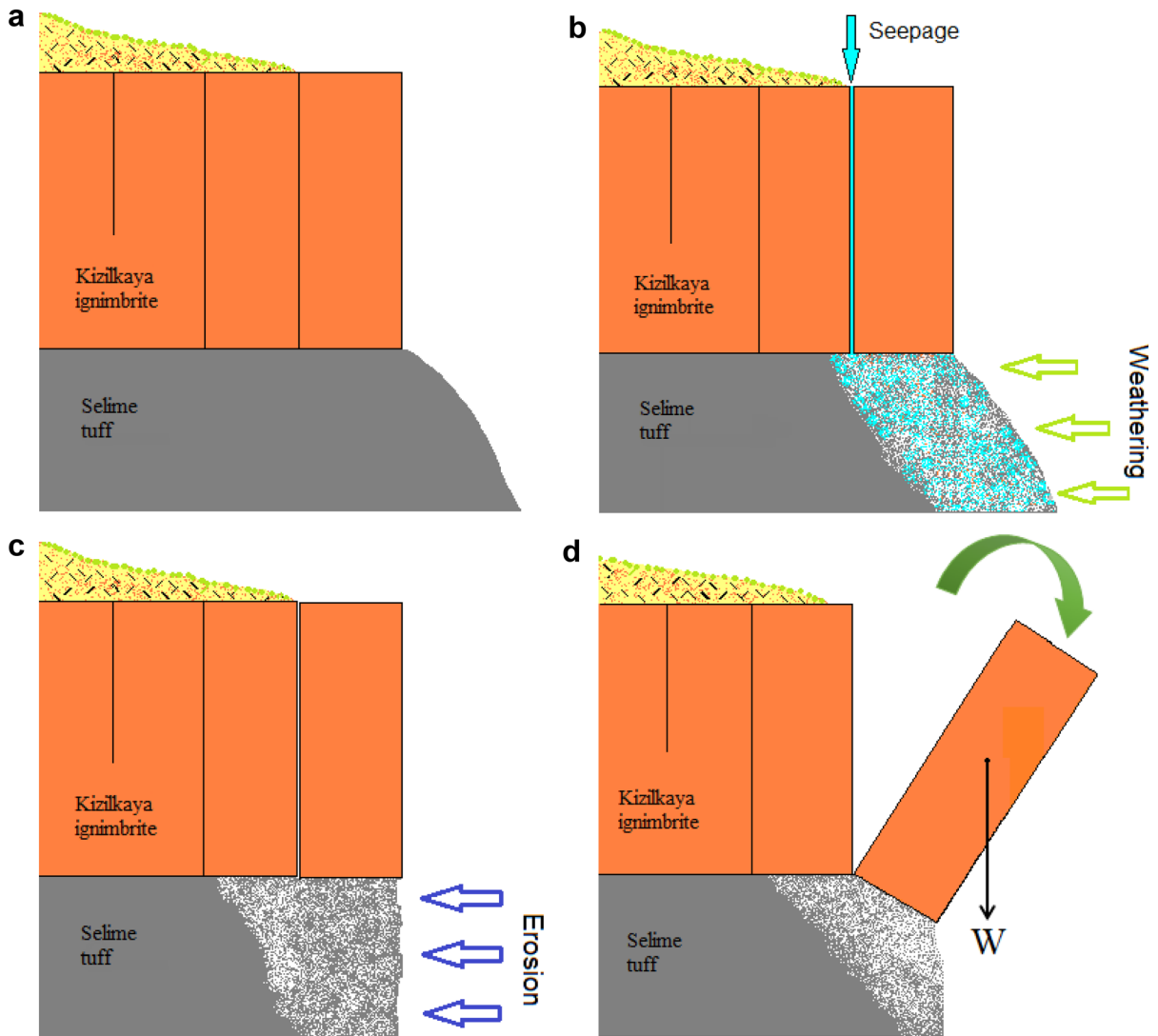
Fig. 3 A simplified model of the secondary toppling failure mechanism in the Ihlara Valley; **a** Original condition of the slope, **b** Seepage of meteoric water through vertical joints into the basal Selime tuff and strength degradation by weathering, **c** Differential settlement and erosion in the toe due to basal weathering, **d** Toppling and slumping of the free block

damaged tuff zone and overturning by self-weight when the center of gravity remains in free space due to removal of support (Fig. 3d).

3 Analysis Methods

3.1 Kinematic Stability Analysis

Geological fractures play a significant role in the development of failures in rock slopes. The dip angle and dip direction of geological fractures with respect to the slope orientation are the most important input parameters in this process (Hoek and Bray 1991). The kinematical analysis is a practical preliminary method to investigate the stability of rock slopes in which the failure is mostly controlled by joint sets in the rock mass (Wyllie and Mah 2004). In a previous study by Sari (2009), detailed discontinuity surveys were conducted on the Kizilkaya ignimbrite outcrop forming the valley cliffs. The scanline surveying of the discontinuities was carried out on the east side of the valley.

A total of 380 measurements, 120 in this study and 260 by Sari (2009) recorded using a Brunton compass and measuring tape in the field was processed using DIPS (version 7.0) software, a stereonet analysis program (Rocscience Inc. 2019b). Three dominant joint sets were identified by the stereonet program using the most highly concentrated areas of the poles (Fig. 4). Set 1 corresponds to the horizontal bedding plane (or ash-fall layer) between Selime tuff and Kizilkaya ignimbrite or different flow units of Kizilkaya ignimbrite. Set 2 and Set 3 are the sub-vertical orthogonal joint sets giving the columnar structure to the valley slope. These two sets were tension fractures formed by cooling and compaction of the rock massif. The equal angle lower hemisphere pole plots in Figs. 5a, d presents the discontinuity-controlled failure modes of the planar, wedge, direct toppling, and flexural toppling, respectively. The dip of the natural slope is very steep, with a mean of 87°, and the dip direction of the slope face on the east side of the valley is 140° SE. In the kinematical analysis, the friction angle of bedding planes (Set 1) is used, which is assumed to be 33° according to Binal (1996).

For the planar sliding in Fig. 5a, there is a possibility of 23.9% for all joint sets, and Set 1 is the critical set leading to planar failure with a percentage of 75.8. When wedge sliding in Fig. 5b is considered, 38.2% of the intersections formed by three sets are susceptible to this type of failure. Direct (block) toppling can be observed among the 13.8% of intersections, and 22.2% of them are also liable to oblique toppling (Fig. 5c). Set 1 forms the base plane of direct toppling for the rock slope. Flexural toppling has a potential of 28.2% for all joint sets, and Set 2 is the most critical one for this type of failure with a percentage of 84.1 (Fig. 5d). The results of the kinematical analysis are presented in Table 2. The kinematic results indicated that wedge and flexural toppling were the primary cause of rock block instability.

3.2 FEM Modeling

3.2.1 Background

A rock mass is a natural material formed by two structural elements: intact rock blocks and fractures.
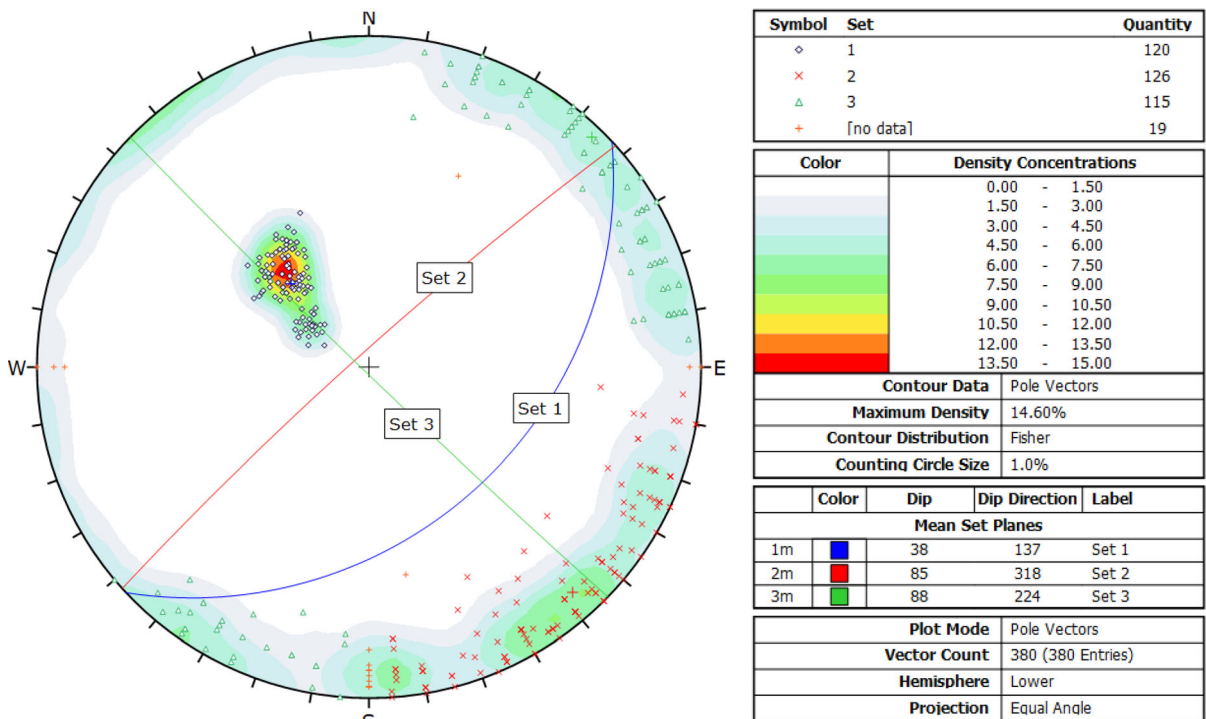
Fig. 4 Equal angle lower hemisphere pole plots of joints in the Kizilkaya ignimbrite with delineated major sets: Set 1:38/137, Set 2:85/318, Set 3:88/224

a

Symbol	Set	Quantity
◇	1	120
×	2	126
△	3	115
+	[no data]	19

Kinematic Analysis	Planar Sliding			
Slope Dip	87			
Slope Dip Direction	140			
Friction Angle	33°			
Lateral Limits	30°			
		Critical	Total	%
Planar Sliding (All)		91	380	23.95%
Planar Sliding (Set 1: Set 1)		91	120	75.83%

Plot Mode	Pole Vectors
Vector Count	380 (380 Entries)
Hemisphere	Lower
Projection	Equal Angle

b

Symbol	Set	Quantity
◇	1	120
×	2	126
△	3	115
+	[no data]	19

Symbol	Feature
▫	Critical Intersection

Kinematic Analysis	Wedge Sliding			
Slope Dip	87			
Slope Dip Direction	140			
Friction Angle	33°			
		Critical	Total	%
Wedge Sliding		27455	71859	38.21%

Plot Mode	Pole Vectors
Vector Count	380 (380 Entries)
Intersection Mode	Grid Data Planes
Intersections Count	71859
Hemisphere	Lower
Projection	Equal Angle

Fig. 5 Kinematical analysis of structurally controlled failures in the Ihlara Valley; **a** Planar sliding, **b** Wedge sliding, **c** Direct toppling, **d** Flexural toppling

The presence of fractures in the rock mass is the leading factor in determining the strength and deformation properties of jointed rock masses. To study the stability of a rock mass, it is necessary to obtain both the strength of the intact blocks and the shear strength of the discontinuities unraveling these blocks (Barton and Choubey 1977). Therefore, in numerical model studies, both rock mass elements should be represented sufficiently for a realistic slope stability analysis.

The failure behavior of blocky/fractured rock masses has been analyzed using different numerical
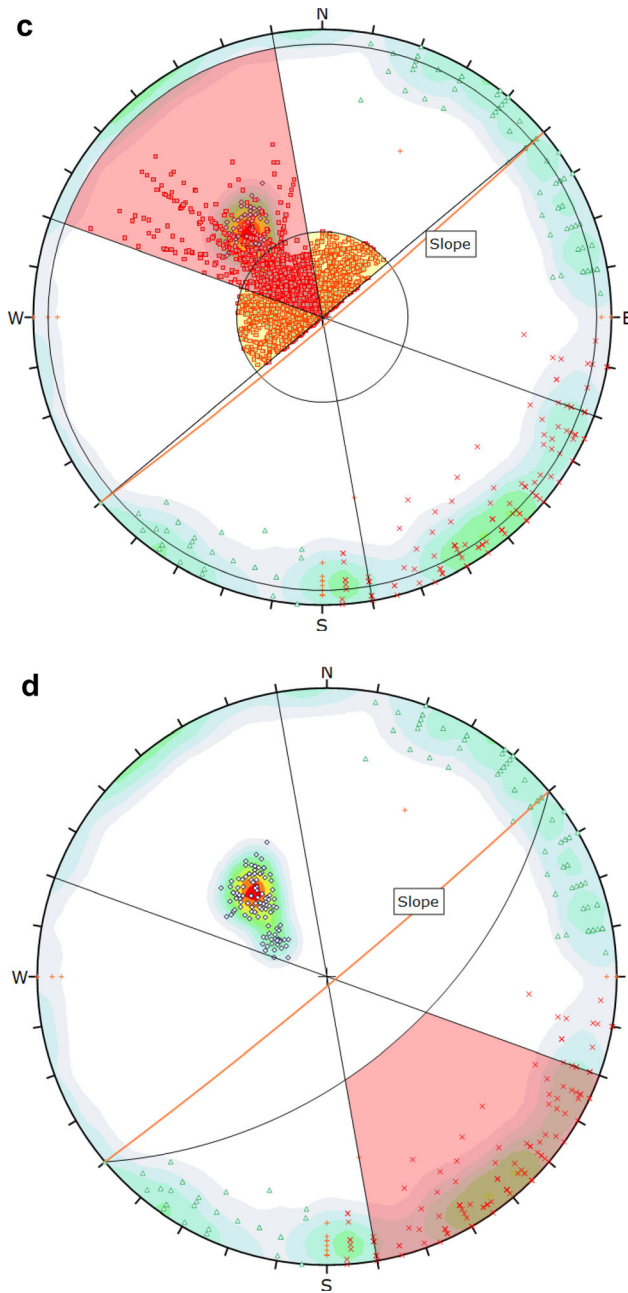
c

Symbol	Set	Quantity
◇	1	120
×	2	126
△	3	115
+	[no data]	19

Symbol	Feature
▪	Critical Intersection

Kinematic Analysis	Direct Toppling			
Slope Dip	87			
Slope Dip Direction	140			
Friction Angle	33°			
Lateral Limits	30°			
		Critical	Total	%
Direct Toppling (Intersection)		9922	71859	13.81%
Oblique Toppling (Intersection)		15927	71859	22.16%
Base Plane (All)		120	380	31.58%
Base Plane (Set 1: Set 1)		120	120	100.00%

d

Symbol	Set	Quantity
◇	1	120
×	2	126
△	3	115
+	[no data]	19

Kinematic Analysis	Flexural Toppling			
Slope Dip	87			
Slope Dip Direction	140			
Friction Angle	33°			
Lateral Limits	30°			
		Critical	Total	%
Flexural Toppling (All)		107	380	28.16%
Flexural Toppling (Set 2: Set 2)		106	126	84.13%

Plot Mode	Pole Vectors
Vector Count	380 (380 Entries)
Hemisphere	Lower
Projection	Equal Angle

Fig. 5 continued

methods, especially continuum and discontinuum based approaches (Bobet et al. 2009). Of the numerical methods employed for the deformation evaluation currently, the group of discontinuous deformation analysis and discrete element methods have been known to be the most suitable to the problems of discontinuous media, particularly blocky rock masses

(Stead et al. 2006; Elmo and Stead 2010; Mas et al. 2011; Mehranpour et al. 2018). Recently, however, it has been shown that the FEMs with explicit joint elements are credible alternatives to discrete element methods (Hammah et al. 2007, 2008, 2009). The method can model a wide range of slope failures, from wedge sliding to toppling and rotational failures at

Table 2 Kinematical analysis results

Failure type	Failure potential, %	Critical set no
Planar sliding	23.95	Set 1
Wedge sliding	38.21	Set 2, Set 3
Block toppling	13.81	Set 1
Flexural toppling	28.16	Set 2

different scales (Hammah et al. 2007). Many studies have validated the accuracy of the FEM- shear strength reduction (SSR) technique for a variety of failure behaviors frequently observed in rock slope cases (Dawson et al. 1999; Griffiths and Lane 1999; Hammah et al. 2005, 2007; Sari 2019). The ultimate advantage of FEM-based SSR analysis is that various failure mechanisms can be automatically captured without prior knowledge about the type, shape, or location of these instabilities (Hammah et al. 2009); thus, it reveals the progress and development of the failure mechanism. Although, in many cases, the FEM-based SSR method is still a substitute to traditional limit equilibrium methods, its ability to capture blocky/fractured rock mass behavior by readily combining slide along joints with damage through intact rock presents numerous benefits in this domain. A combined continuum-joint interface model is the most suitable for blocky or very blocky rock mass structure since it can replicate the actual field state (Pain et al. 2014).

3.2.2 Defining Material Properties

It is extremely important to consider the correct failure criteria with reliable input data for jointed rock masses when performing a slope stability analysis (Sari 2019). For this purpose, rock material and joint properties of the rock massif forming the valley cliffs were extracted from the literature, and considerable effort was exerted to gather the necessary input data for the numerical modeling study. For this purpose, the works of Binal (1996), Sari and Çömlekçiler (2007), Sari (2009), and Taşpınar (2015) were carefully evaluated. Accordingly, the strength and stiffness parameters of the geologic units outcropping in the Ihlara Valley were determined and given in Table 3. Moreover, the rock masses' failure envelopes were illustrated in

Fig. 6 for the major-minor principal stress space and shear-normal stress space, respectively. The generalized Hoek–Brown failure criterion (Hoek et al. 2002) was employed to characterize rock mass behavior, and the Mohr–Coulomb slip criterion was used to define joint behavior in the FEM models. The elastic-perfectly plastic constitutive model was utilized to mimic the failure behavior of the rock mass. The residual GSI_r values of the geologic units were obtained considering Cai et al. (2007) suggestions.

3.2.3 Building FEM Models

Two-dimensional (2-D) numerical modeling was undertaken using the FEM software RS2 (Rocscience Inc. 2019a). This software has been extensively utilized in several slope studies for the numerical modeling of rock stability using the SSR technique. In these studies, the SSR technique is used to perform slope stability analysis in stages until failure occurs by reducing the rock or soil shear strength properties (i.e., c and ϕ). The safety factor (FoS) can be expressed as the factor by which the original shear strength parameter is divided to initiate failure in the slope. RS2 executes a regular search for strength reduction factor (SRF), starting from a value of unity to the value that brings the slope to the verge of failure. The critical value of SRF found in the process is called the FoS (Dawson et al. 1999; Griffiths and Lane 1999; Hammah et al. 2005, 2007; Roosta et al. 2005; Shen and Karakus 2014; You et al. 2018).

The secondary toppling mechanism in the Ihlara Valley might be more complex than that illustrated schematically in Fig. 3. Also, artificial caves and churches at the slope base are a further factor that possibly promotes instability in the valley. For a more comprehensive analysis and support design, special software that considers the time-dependent progressive failure and differential settlements at the base of overlying rigid blocks due to basal weathering is needed. However, to simplify the problem and facilitate an approximate numerical solution, the effects of artificial caves on the failure process and differential settlement induced by the ignimbrite blocks were not separately considered in the subsequent analysis. For the analysis, three FEM models given in Fig. 7 were built using the RS2 program. The FEM models are designed to capture the stages of progressive failures naturally occurring in the valley slopes before any

Table 3 Rock material and rock mass parameters defined in the FEM models

Input parameters	Hasandagi ashes	Kizilkaya ignimbrite	Selime tuff	Weathered tuff	Joint set 1	Joint set 2	References
γ_d (kN/m³)	16.2	19.6	17.5	15.0	–	–	Binal (1996); Sari and Çömlekçiler (2007); Sari (2009); Taşpınar (2015)
UCS (MPa)	5.5	46.06	6.68	2.82	–	–	
BTS (MPa)	0.69	3.78	0.58	0.35	–	–	
c (MPa)	–	–	–	–	0.25 (0)	0.5 (0)	
ϕ (°)	–	–	–	–	33 (20)	35 (25)	
GSI (%)	45 (24.6)*	65 (27.2)	50 (25.6)	35 (21.9)	–	–	
m_i	8 (5)	13 (9)	10 (6)	7 (4)	–	–	
E_t (GPa)	3.50	12.64	6.25	2.78	–	–	

*Peak (residual); γ_d, dry unit weight; UCS, uniaxial compressive strength; BTS, Brazilian tensile strength; c, cohesion; ϕ, friction angle; GSI, geological strength index; m_i, Hoek–Brown constant; E_t, Young's elastic modulus

human intervention. The following assumptions are implemented in the FEM analysis:

- The top and right boundary, defining the topography of the 2-D section, is set as unconstrained, while the bottom and left model sides are fixed for both vertical and horizontal displacements.
- Stress field properties are set to gravitational only. Since the actual field measurements were not available, the vertical and horizontal stresses were assumed to equal each other (i.e., hydrostatic conditions with k = 1.0). Evans (1981) found that horizontal stresses could be greater than vertical stress in such cases, and it shows a pronounced effect on the failure process.
- The geometry is discretized with a 6-noded uniform triangular mesh (3667 nodes/1775 elements).
- The joints in the FEM models are included to represent the structural discontinuities observed in the Kizilkaya ignimbrite (see Fig. 4). For the 2-D plane strain case, joint Set 2 is described as in-plane finite length uniformly distributed vertical joints. Joint Set 1 is defined as the bedding planes between tuff and ignimbrite. Joint Set 3 is not incorporated in the FE analysis since it is located outside the plane (Fig. 4).

- There is no tensile strength across the joints at the back of the ignimbrite columns.
- The dimension of blocks dividing a rock mass into separate pieces is an important element in the FEM analysis. Its shape and size are determined by geometrical parameters such as the spacing, number of sets, and discontinuity orientation. The spacing of sub-vertical orthogonal joint sets (Set 2 and Set 3) in the Kizilkaya ignimbrite ranges from 2.0 to 5.25 m with an average of 3.44 m. For this purpose, the rectangular blocks' width in the models is set equal to the spacing of joint Set 2.
- The height of the rectangular blocks is determined based on the average thickness of the Kizilkaya ignimbrite in the valley, which is 25 m.
- The weathered zone in the tuff layer is represented by reduced strength and stiffness values, and it extends approximately halfway across the second block's base width in the slope.
- From a toppling point of view, the most crucial factor is the ratio of block width (W) to block height (H) (Evans 1981). In the study, the effect of the W/H ratio on the toppling failure mechanism is also evaluated. Given the inherent variability of the joint spacing, different W/H ratios of the rectangular blocks are considered in the numerical analysis. Three different block sizes are chosen to represent the range of spacing values of joint Set 2
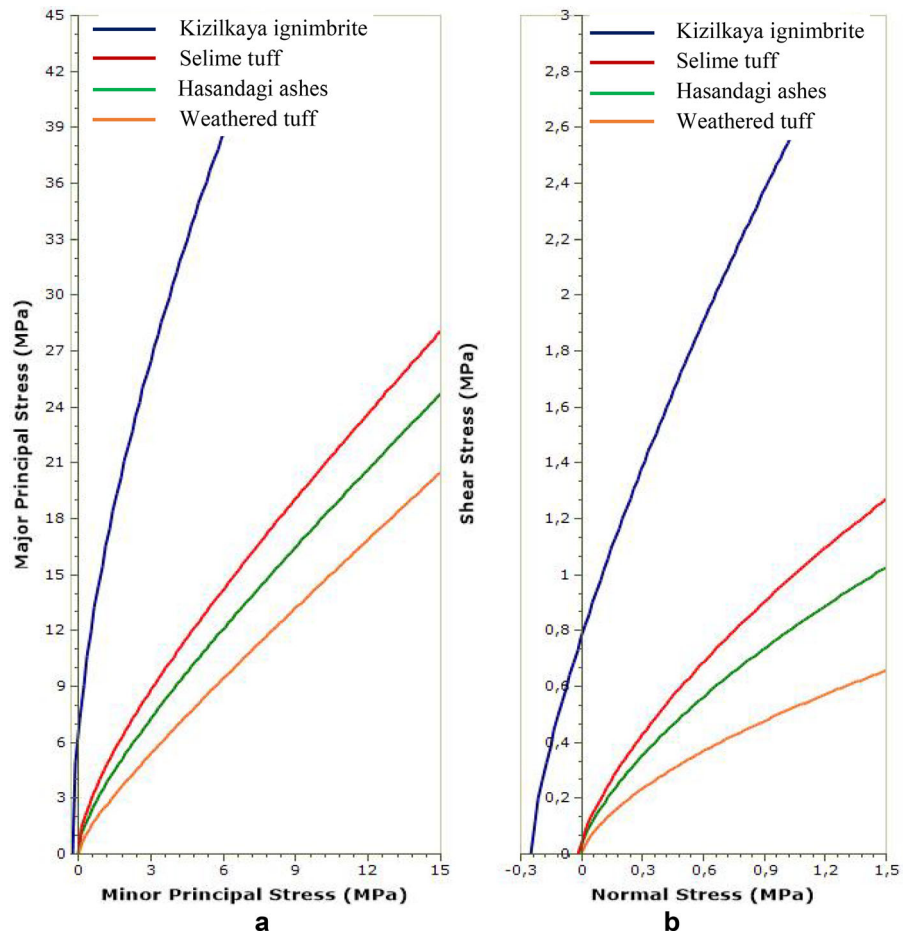
Fig. 6 a Major principal stress-minor principal stress envelope, b Shear stress-normal stress envelope for the rock masses in the Ihlara Valley
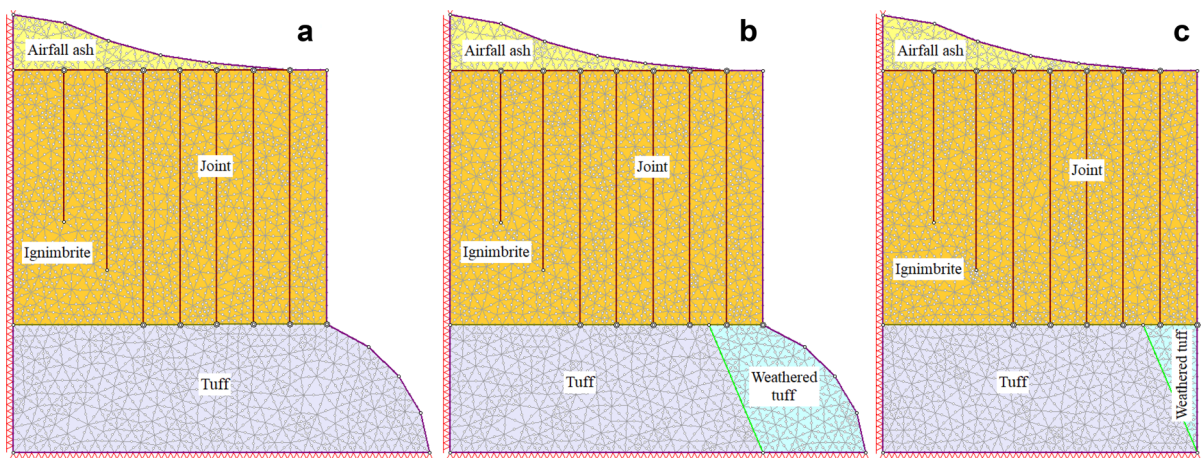
Fig. 7 Three stages of FEM models simulating the toppling failure in the Ihlara Valley for Block B (W = 3.5 m); a Stage 1-original slope geometry, b Stage 2- strength degradation of soft tuff underneath due to water infiltration and weathering, c Stage 3-removal of the toe as a result of erosion in the weathered tuff zone

as Block A for minimum (W = 2.0 m), Block B for median (W = 3.5 m), and Block C for maximum (W = 5.25 m).

- Only dry conditions (water pressure in the joints being negligible) and static loads (i.e., no dynamic loading) are realized in the numerical analysis.

4 Results and Discussion

Figure 8 presents the SRFs calculated from the three different secondary toppling failure stages for three different block sizes in the FEM analysis (in total, nine separate FEM models). It was seen that as the stages of failure propagate in the slope, the SRFs decreased subsequently from 2.05 to 0.45. The rock slopes' overall stability was acceptable in Stage 1, having SRF values greater than 1.9. For the cases in Stage 2, the slopes with SRF of 1.0–1.3 were marginally stable and required immediate treatment by appropriate corrective measures. On the other hand, Stage 3 represents a special condition in the slope where it was too late to install a support system since the SRF values were considerably below 1.0 for the evaluated block sizes.

The results of FEM analysis in Fig. 8 also revealed that the W/H of the blocks considered in this study did not significantly affect slope stability when similar SRF values were taken into account. For instance, for Block A, the SRF was calculated as 1.91 in Stage 1 (Fig. 8a). On the other hand, the SRF was raised to 1.99 in Block C (Fig. 8c). Changing W/H from (2.0/25 = 0.08) to (5.25/25 = 0.21) caused an insignificant increase in the computed SRF values. Similarly, an insignificant increase in the slope stability was also detected for Block B with an SRF of 2.05 (Fig. 8b). Similar observations were also noticed for the remaining block sizes and failure stages evaluated in the FEM models. Contrary to expectations, there was no specific trend in the computed SRF values due to increased W/B for the simulated block sizes. Only in the last stage of the failure process, a marginal increase of the SRF was observed as the W/H of block increases. In this stage, SRF was increased from 0.45 to 0.48 as the W/H increases.

The underlying mechanism of toppling in the valley slopes needs to be correctly explored to design an accurate rock support system. For this purpose, possible mode of failures developing in the slope

was carefully examined by considering the three separate stages of FEM models in Fig. 8. When the total displacement counters were taken into account in Stage 1, a circular shear failure in the slope was the reason for the instability since the circular slip surface developed in the basal continuous tuff mass seems to be the dominant factor (Fig. 8a). This finding is following the analytical solution proposed by Haghgouei et al. (2020). In Stage 2, rotation of the free blocks in the upper part of the slope was the major cause of failure due to differential settlement after basal weathering (Fig. 8b). In Stage 3, back tilting of the detached blocks over a plane of weakness in the basal tuff layer played a critical role in the failure mechanism (Fig. 8c).

4.1 Optimal Support Selection and Design

Certain preliminary information about the types of supports suitable to the condition of rock structure in the valley and their optimum configurations should be considered. The desired sort of support or reinforcement components and the desired pattern and installation sequence depend on the in-situ ground conditions, the rock mass environment, and the excavation type (Hoek 2008). RS2 program includes a wide range of support choices; (1) end anchored, (2) fully bonded, (3) plain strand cable, (4) swellex/split set, and (5) tiebacks. Among these bolt types, fully bonded rock bolts are the most suitable when the blocky structure of rock mass in the valley was considered. Rock bolt is a support scheme widely applied in mining and civil engineering works, particularly for subsurface excavations due to their ease of application, efficiency and rather low costs (Stillborg 1994).

Fully bonded rock bolts in RS2 are divided into two-dimensional bolt elements according to where the bolts pass the finite element mesh (Fig. 9a). These bolt elements act independently of each other. Neighboring fully bonded bolt elements do not directly affect each other but only indirectly through their influence on the rock mass. Additionally, the strength and deformation of the bolt-grout and grout-rock boundaries are not considered by the program since the bolt is supposed to endure fully bonded to the rock up until damage occurs. In this respect, fully-grouted rock bolts undergo damage in the FEM model once the axial force acting on the bolt section surpasses the bolt's

a Block A (W=2.0 m)

b Block B (W=3.5 m)

c Block C (W=5.25 m)
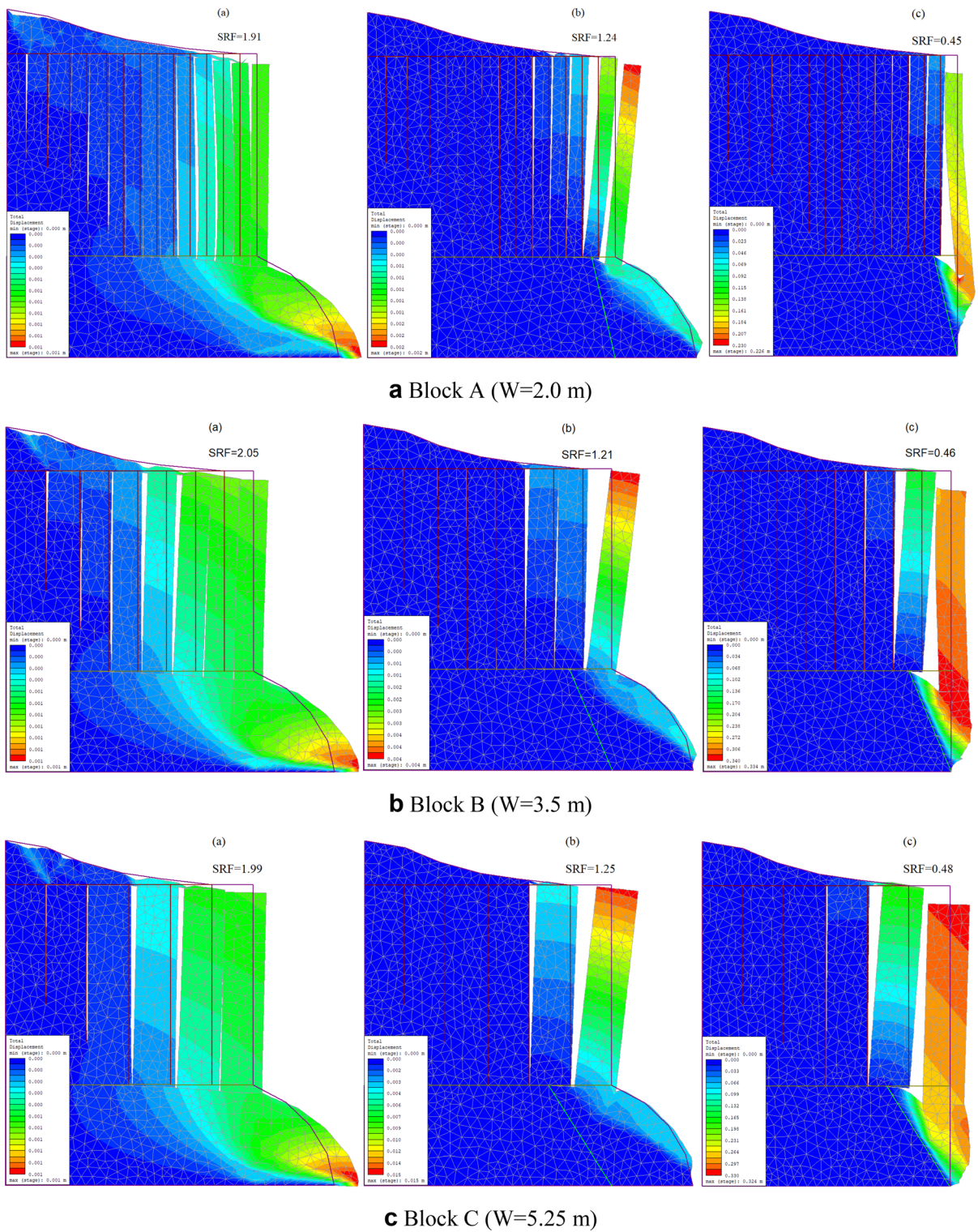
Fig. 8 Change of SRFs in the FEM models simulating the total displacement counters for three separate stages of the failure in the rock slope with **a** Block A, **b** Block B, and **c** Block C
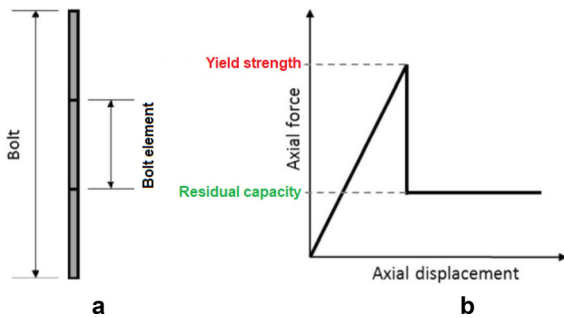
Fig. 9 **a** Fully-bonded rock bolt model in RS2 software, **b** Bolt failure criteria (modified from Vlachopoulos et al. 2020)

axial capacity. At this stage, the bolt section is allocated a residual capacity (Fig. 9b). Although it is possible to initially approximate the bolts' pattern capable of supporting the rock stratum using this bolt functionality in RS2, it greatly simplifies the mechanism related to axially loading fully-grouted rock bolts (Vlachopoulos et al. 2020).

The main function of a rock bolt is to prevent the collapse of rock blocks susceptible to structurally controlled instability by fixing them to an adjacent stable block or rock stratum for stabilization. Pattern bolting comprises the implementation of rock bolts or cables in a fixed configuration that is aimed to support the entire rock column in much the same way as reinforcing steel acts in reinforced concrete (Hoek 2008). In principle, the total tensile capacity provided by the installed rock bolts must be enough to carry the weight of a single block. In the analysis, 250 N load capacity 25 mm diameter rock bolts were implemented to provide adequate support. Accordingly, the following calculations were executed to find the minimum number of rock bolts (N) necessary for each block.

For W = 2.0 m block (Block A);

$$W_t = H \times L_b \times W \times \gamma_d = 25 \times 2.0 \times 2.0 \times 19.6 = 1,960\,\text{kN}, \tag{1}$$

where W_t is the weight of a single block with a height H (m), length L_b (m), width W (m) and unit weight γ_d (kN/m³). Using rockbolts each with a 250 kN load capacity, the installation should be;

$$N = 1,960 \div 250 \cong 8\,\text{bolts}. \tag{2}$$

For W = 3.5 m block (Block B);

$$W_t = 25 \times 3.5 \times 3.5 \times 19.6 = 6,000\,\text{kN}, \tag{3}$$

$$N = 6,000 \div 250 \cong 24\,\text{bolts}. \tag{4}$$

For W = 5.25 m block (Block C);

$$W_t = 25 \times 5.25 \times 5.25 \times 19.6 = 13,505\,\text{kN}, \tag{5}$$

$$N = 13,505 \div 250 \cong 57\,\text{bolts}. \tag{6}$$

Figure 10 shows schematically grid pattern of the fully-grouted rock bolts for the different block sizes. Another critical design parameter in rockbolt selection is the rockbolt length. For an underground excavation, Barton (1989) recommends the minimum rockbolt length for the sidewalls as;

$$L = 2 + 0.15H \tag{7}$$

where H is the excavation height in meter. For our case, assuming the block height as excavation height, the required minimum rockbolt length is found as L = 2 + 0.15 × 25 = 5.75 m.

The main features of the rock bolts according to the block sizes modeled in the FEM analysis are presented in Table 4. Twenty-four 5.75 m long, 250 kN load
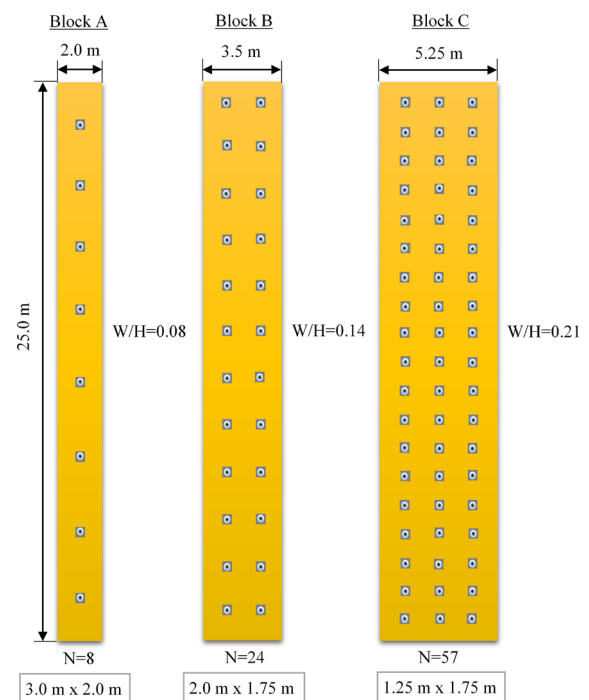
Fig. 10 The grid pattern of fully-bonded rock bolts shown schematically on the various block sizes forming the valley slopes

Table 4 The block dimensions and fully-bonded rock bolt specifications in the numerical models

Input parameter	Block A	Block B	Block C
Block height, H (m)	25	25	25
Block width, W (m)	2.0	3.5	5.25
Block length, L_b (m)	2.0	3.5	5.25
No. of bolts, N	8	24	57
Bolt diameter, Ø (mm)	25	25	25
Bolt modulus, E (GPa)	200	200	200
Tensile capacity, T_p (kN)	250	250	250
Residual tensile capacity, T_r (kN)	25	25	25
In-plane spacing, X (m)	3.0	2.0	1.25
Out-of-plane spacing, Y (m)	2.0	1.75	1.75
Bolt length, L (m)			
L = 1.5 W	3.0*	5.25*	7.875
L = 2.5 W	5.0*	8.75	13.125
L = 3.5 W	7.0	12.25	18.375
L = 1.5 W/Cos15°	3.1*	5.45*	8.15
L = 2.5 W/Cos15°	5.2*	9.05	13.6
L = 3.5 W/Cos15°	7.25	12.70	19.05

*Cases not satisfying minimum bolt length criteria in Eq. (7)

capacity rock bolts in a 2.0 m × 1.75 m grid pattern may be required for a typical block of W = 3.5 m in the rock slope. In the FEM models, the rock bolts are assumed to be passive, meaning there is no pretension. Previous research has shown that exerting pre-load on the bolt is not always advantageous for all situations (Stillborg 1994; Hoek 2008). Since in most cases, the extent of a bolt inserted within the rock mass is long enough to establish adequate shear strength to support the loads it can sustain during its life (Haas 1975). However, some bolt length applications in Table 4 were not obeying the minimum bolt length criterion given in Eq. (7). The rock bolt lengths in Block A and Block B need to be extended at least up to the third and second blocks in the slope to meet the criterion.

4.2 Failure Analysis after Support Installation

In this section, the support configuration suggested in Table 4 was realized on the FEM models. It was expected to observe some improvements in the SRF values after the support installation. In the FEM models, the rock bolts are implemented mainly to anchor potentially unstable rock blocks in place. The analysis undertaken by Evans and Valliappan (1981) indicated that the rock bolts or anchors must be seated far back into the slope and should preferably be

located near the top of the slope. This means that a stable stratum outside of the rock column's influence zone is needed to extend rock bolts. A possible solution that should be considered in this case is to lengthen the bolts; thus, more blocks behind the rock face are fastened together in situ. However, there should be an optimal bolt length sufficient to stabilize the affected blocks in the slope. For an efficient support design, FEM analysis was conducted on different bolt length configurations given in Table 4. There are generally two options available for support implementation in the rock slopes; first, installing rock bolts horizontally and installing them at a certain degree to horizontal. Some researchers (Stillborg 1994; Hoek 2008) pointed out that the application of support with a certain inclination into slope may improve the rock bolts' expected capacity. The literature usually suggests 15°–30° as a reasonable choice for the inclination (Hoek 2008). Figure 11 shows FEM models with three different stages for an inclined bolt application with a length of L = 3.5 W/Cos15° in the slope.

The change of SRF values for different rock bolt length configurations is presented in Fig. 12 for Block B. The results clearly showed that as the length of rock bolt increases in the FEM models, the SRF marginally increases. Stage 2 seems to be the most suitable stage to install supports among the evaluated three stages
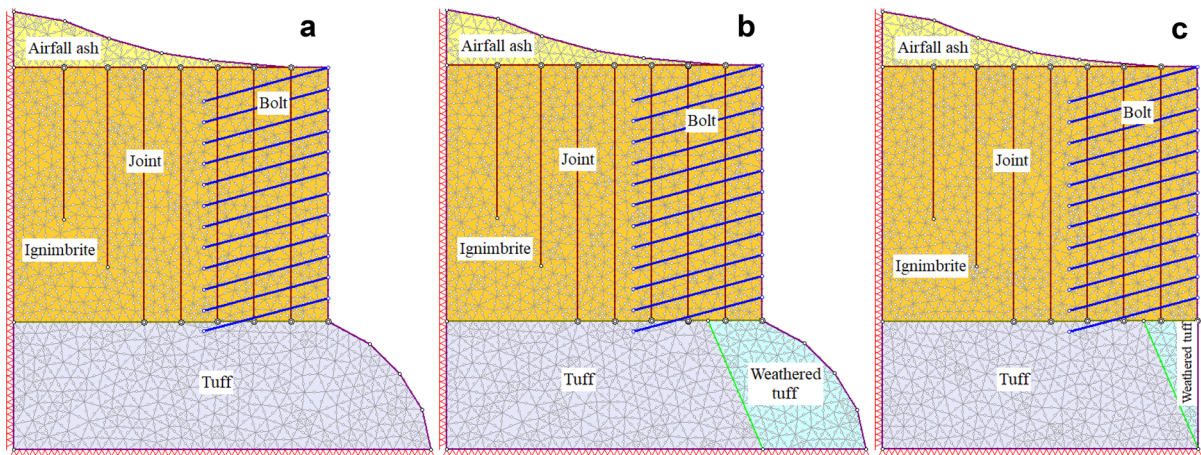
Fig. 11 FEM models after installation of inclined rock bolts in Block B for three possible stages of failure in the slope

due to a relevant increase in SRFs in the rock slope. In this stage, the slope failure was mainly controlled by the toppling of detached blocks due to differential settlement at the base of the blocks. The concentration of total displacement counters on the top of the detached blocks is a sign of toppling movement. Although the highest relative increase in SRF after bolt installation was observed in Stage 3, it would be too late to install rock bolts for a slope at this stage of failure since the new calculated SRF values were still less than 1.0. Stage 1 was the least affected case from the bolt installations. At this stage, the slope failure was initially started due to a circular shear failure in the underlying tuff zone. Installing rock bolts in this failure stage would cause the failure type to shift from a circular one to the toppling of blocks. A fascinating outcome of the FEM analysis was revealed in the last stage of failure for the case of a bolt length of L = 3.5 W as seen in Fig. 12d. All the blocks in the slope were restrained in place due to extended bolt lengths, although an SRF of 0.67 was executed for the model. Initially, the slope failure was a result of sliding the detached blocks over the weak tuff layer. However, as the bolt length increases, the failure was caused by the damage zone developed in the underlying weathered tuff zone since no movement occurs in the bolted blocks above. Overall, these findings suggest that the rock bolts should be extended into the second and third rigid self-supporting blocks, especially in the last two stages of the slope failure. The change of calculated SRFs for various block sizes and

bolt length configurations is given together in Fig. 13 for different stages of FEM models.

As shown in Fig. 14a, if no bolt model case is taken as a reference point in the analysis, the most significant SRF value change was observed with a 55.6% increase in Block A at Stage 3. It means that the thinner the block, the more disposed to toppling mode of failure in the slope. Hence, the thinner blocks show the greatest response to the bolt installations. Similarly, the last stage (i.e., Stage 3) is the most sensitive to the support installations among the evaluated failure stages. It can be discerned in Fig.14a, b that as the bolt length increases, the SRF value and the % change with respect to no bolt case also increase. This indicates that it would be advantageous to extend rock bolt length if one expects to improve stability in the valley slopes. However, Stage 1 is the least affected case from the bolt installations by providing more blocks to move together. This is a specific stage in the slope where the instability mostly took place in the underlying weak rock mass due to a circular shear failure. The same figure also shows that a thicker block is less sensitive to supporting installations, and the reason for this effect may be attributed to the number of active and passive blocks taking part in the failure process. Whether the rock bolts were installed as horizontal or inclined, there was a minimal change between SRF values with a similar trend, as shown in Fig. 14.

The total displacement counters with the calculated SRF values are displayed in Fig. 15 for three separate failure stages of Block A in the slope. To better understand the failure response of the rock bolts within
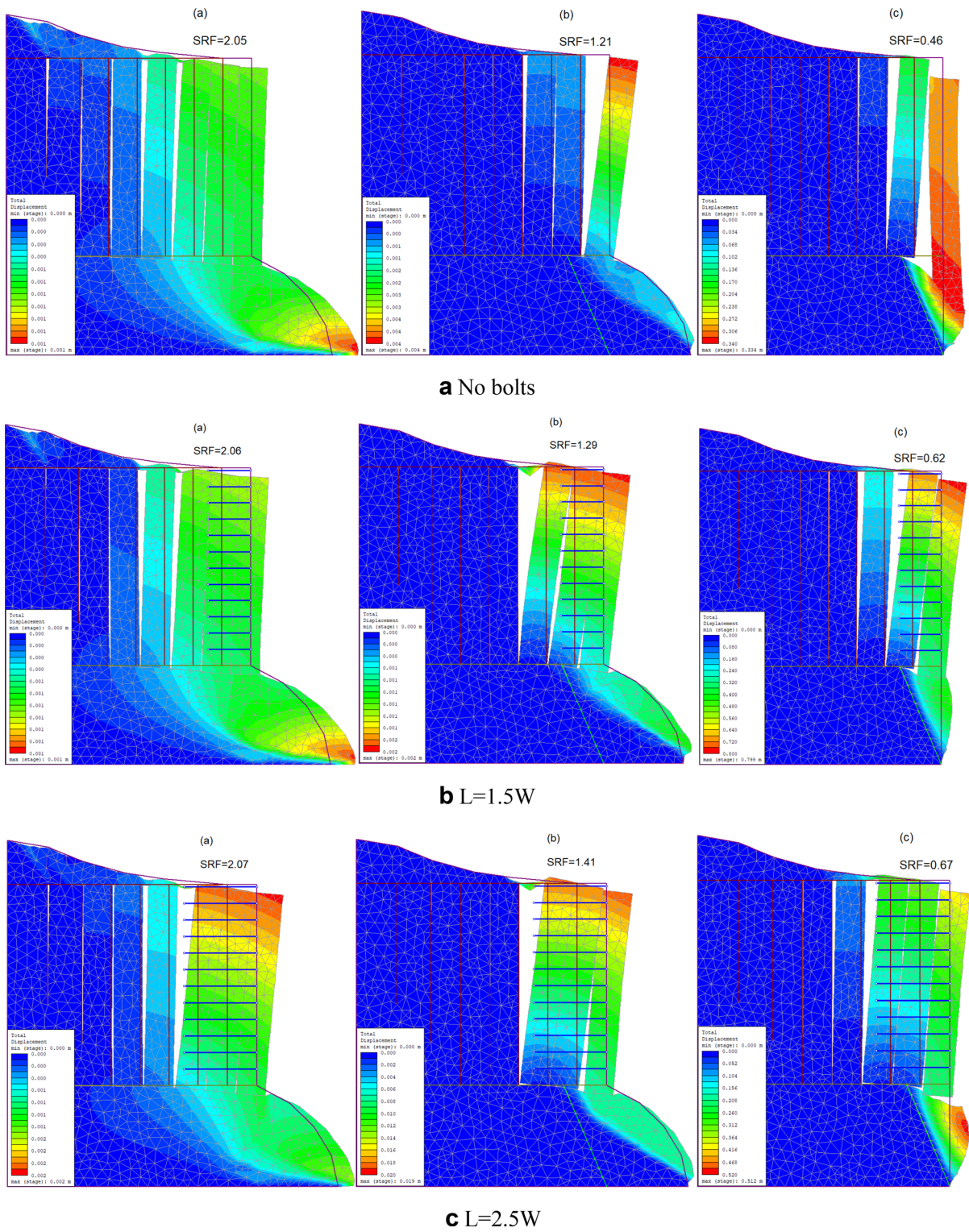
Fig. 12 Change of SRF values for different rock bolt length applications in Block B for three separate stages of the failure, **a** No bolts, **b** L = 1.5 W, **c** L = 2.5 W, **d** L = 3.5 W
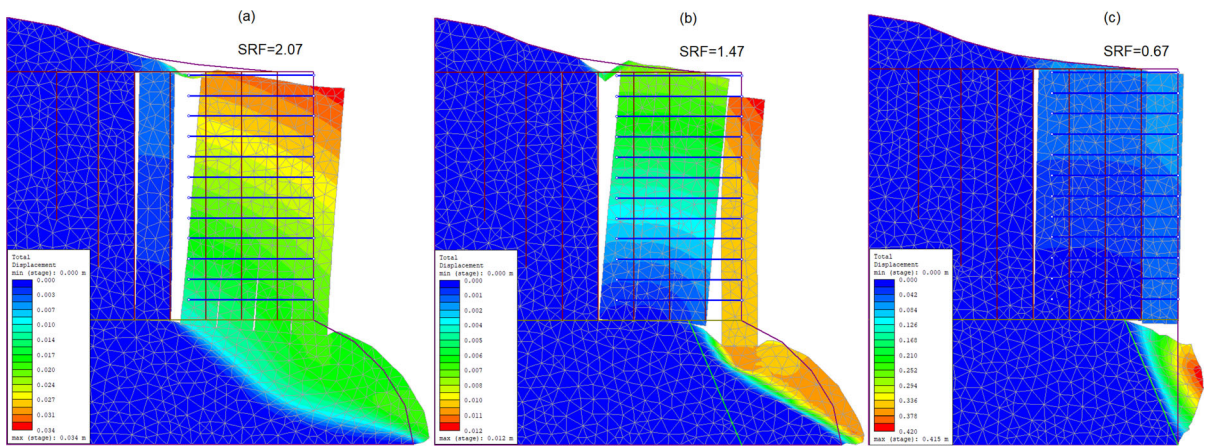
d L=3.5W

Fig. 12 continued
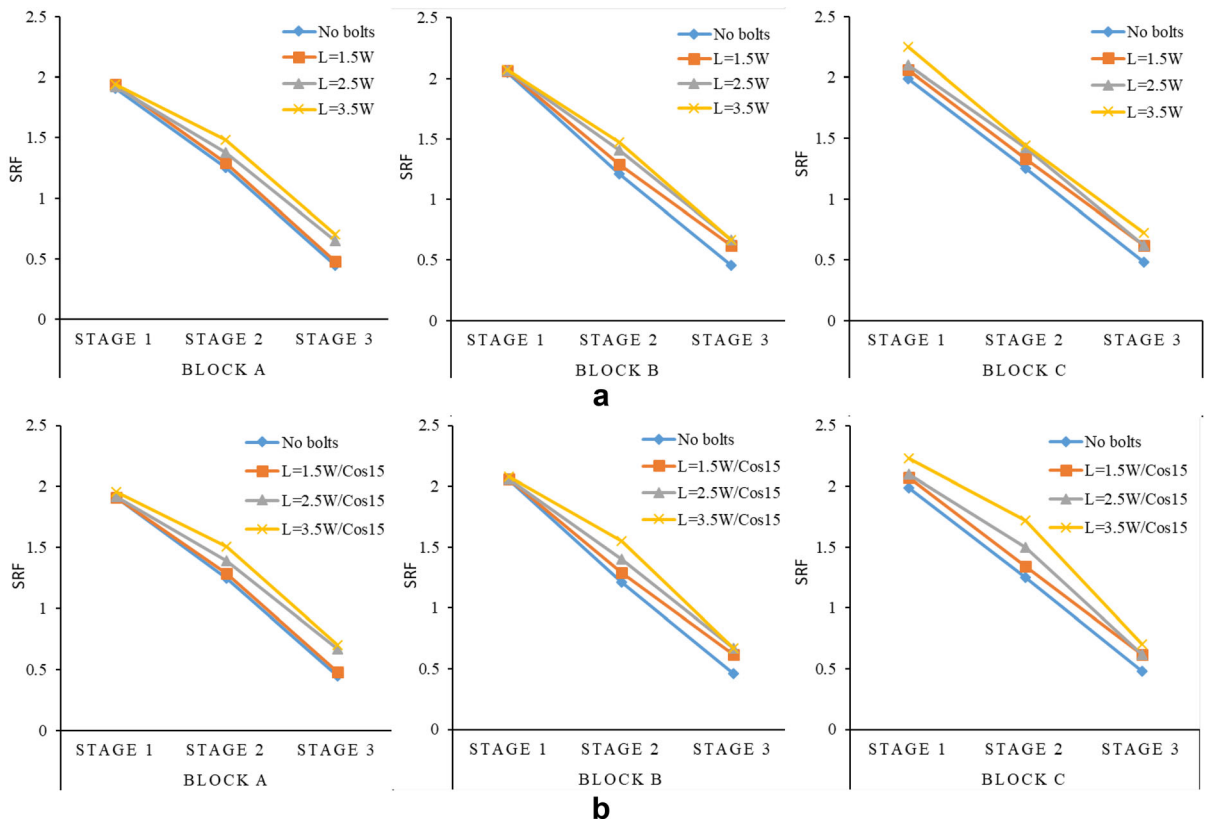
Fig. 13 Change of SRF values after bolt installations in the FEM models, **a** Horizontal, **b** Inclined applications

this arrangement of the blocks, axial force distribution along the bolt length is plotted in Fig. 16. Being aware of which part of the bolt is subjected to stress or damage can be valuable information concerning

appropriate support selection and design. In principle, the axial force versus distance plot reflects the interaction between the bolt element and joints in the rock mass. In Stage 1, since no movement occurred in
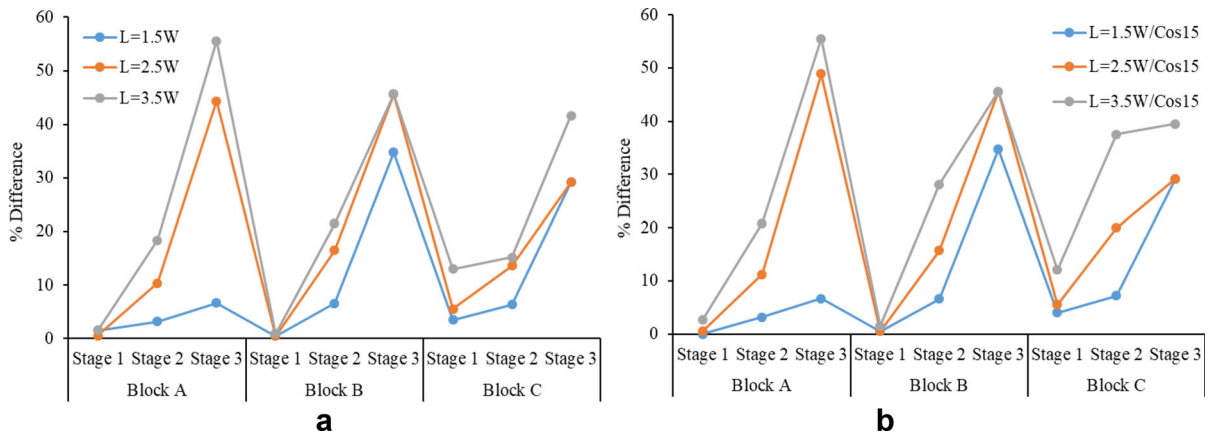
Fig. 14 Percentage change of SRF values after bolt installation in the FEM models, **a** Horizontal, **b** Inclined applications

the above blocks (the instability being mostly due to circular shear failure in the basal tuff mass), the rock bolts in the slope did not sustain significant axial force. A maximum axial force of 18 kN was observed on bolt #10 (Fig. 16a). In Stage 2, since the blocks were subjected to some rotational movements due to differential settlements at their base, some bolts experienced an axial force that was almost half of the bolt capacity. In this stage, the maximum axial force was measured as 130 kN in bolt #10 and bolt #9 on the first and second intersection points of the joints at the bottom of the slope (Fig. 16b). In Stage 3, the bolts still sustained an axial force close to half of the bolt capacity; however, as the bolts' location on the block moves from the bottom to the top, the axial force along with the bolts decreases. Similarly, as the bolt's length extends from the free face into the inner blocks, the bolts' axial force at intersection points with joints also drops. Similar trends were also depicted for the other block sizes and bolt length configurations of the FEM models, but due to limited space, the results are not covered in detail in this study.

5 Conclusions

In this study, one of Turkey's protected areas was subject to investigation due to its natural columnar structure of rock masses surrounding the slope. The toppling failure of jointed rock blocks exposed in the Ihlara Valley was analyzed using numerical methods. The study provided valuable insights into the remedial studies to be undertaken in the future to safeguard this

important natural and cultural heritage. The following conclusions can be derived from the numerical study:

- Depending on the slope failure stages, different modes of failure were detected in the numerical models.
- Although the circular shear failure of the basal soft rock mass was dominant in the early stages, in the later stages, rotation or slumping of the detached blocks in overlying hard rock mass due to differential settlement and undercutting was the main reason for the failure.
- Rock bolts should be installed with sufficient length in the later stages of failure so that at least two adjacent blocks of overlaying rock mass could stay together in place.
- The bolts' arrangement does not significantly affect increasing the amount of SRF and decreasing the displacement of the blocks. Both horizontal or inclined bolt applications increased the SRF marginally.
- Although the FEM models seem to be a feasible solution for a slope design tool in a jointed medium, it is necessary to improve the program's constitutive model to accurately capture the interface between a bolt and joint elements after support installation.
- As presented in this study, the Ihlara Valley slopes may require immediate treatment by rock bolting. However, alternative techniques, such as improving the mechanical properties of basal soft tuff, sealing of vertical joints by grouting to increase shear strength along the discontinuities, and opening suitable diverting channels at the crest of the
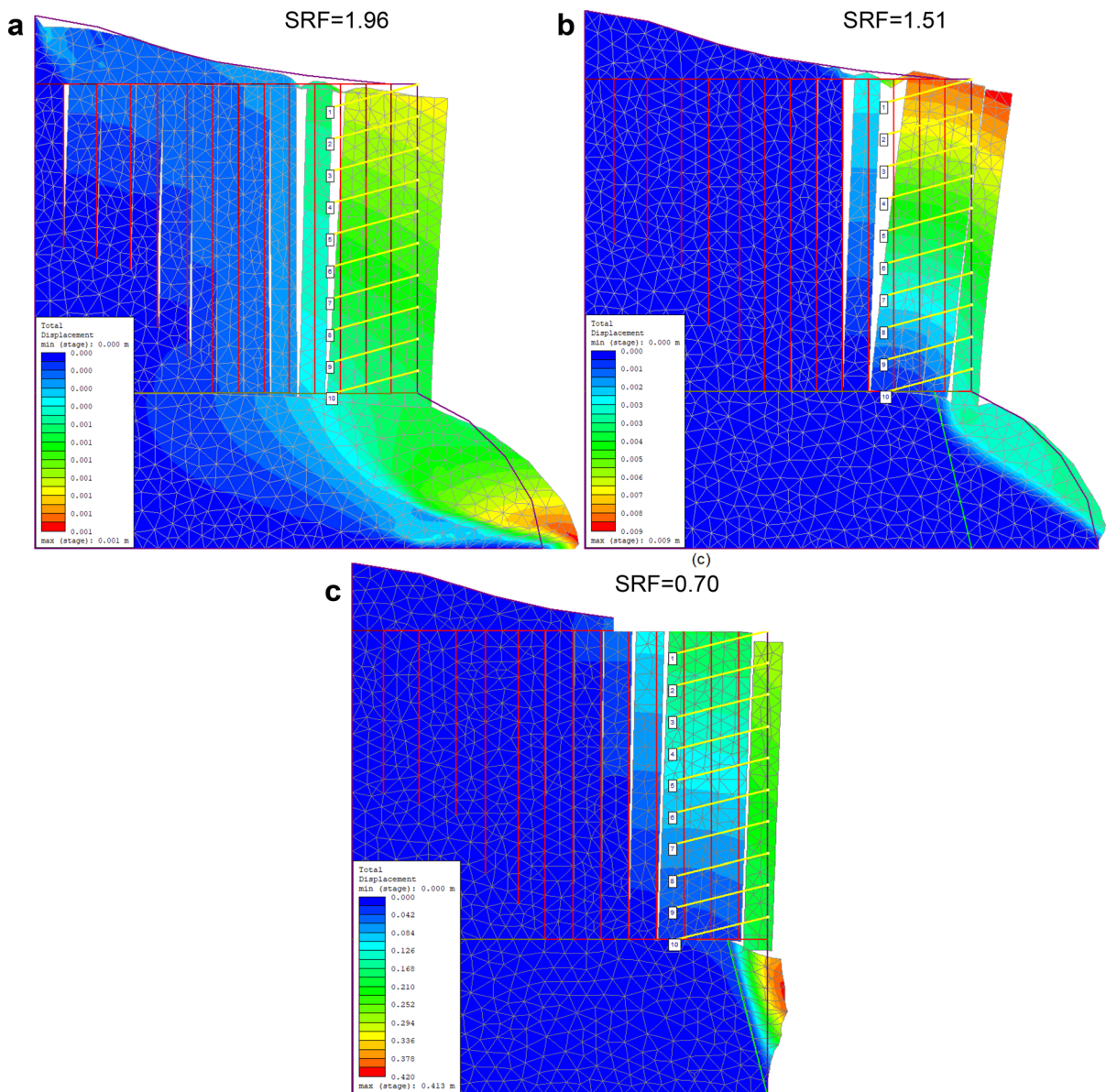
Fig. 15 Calculated SRF values and the distribution of bolts in Block A for a length of L = 3.5 W/Cos15° in three different stages of the failure, **a** Stage 1, **b** Stage 2, **c** Stage 3

slope to prevent seepage of runoff water may be more economical options in the long term.

Since the effect of pre-existing joints on the rock mass response is more likely to be investigated using more advanced numerical methods such as discrete element methods due to the problem's scale, future work should be directed to accurately capturing the failure process and evaluating its sensitivity to the changing input parameters in discontinuum-based models. Furthermore, the impact of artificial cavities, earthquake loading, and water pressure in the joints should be extensively studied since the rock slopes are currently at their very limits of failure.

Fig. 16 Axial force vs. distance plot of rock bolts on Block A for the three separate stages, **a** Stage 1, **b** Stage 2, **c** Stage 3 of the failure (see Fig. 15 for the exact location of bolts on the block; bolt #1 at the top, bolt #10 at the bottom)
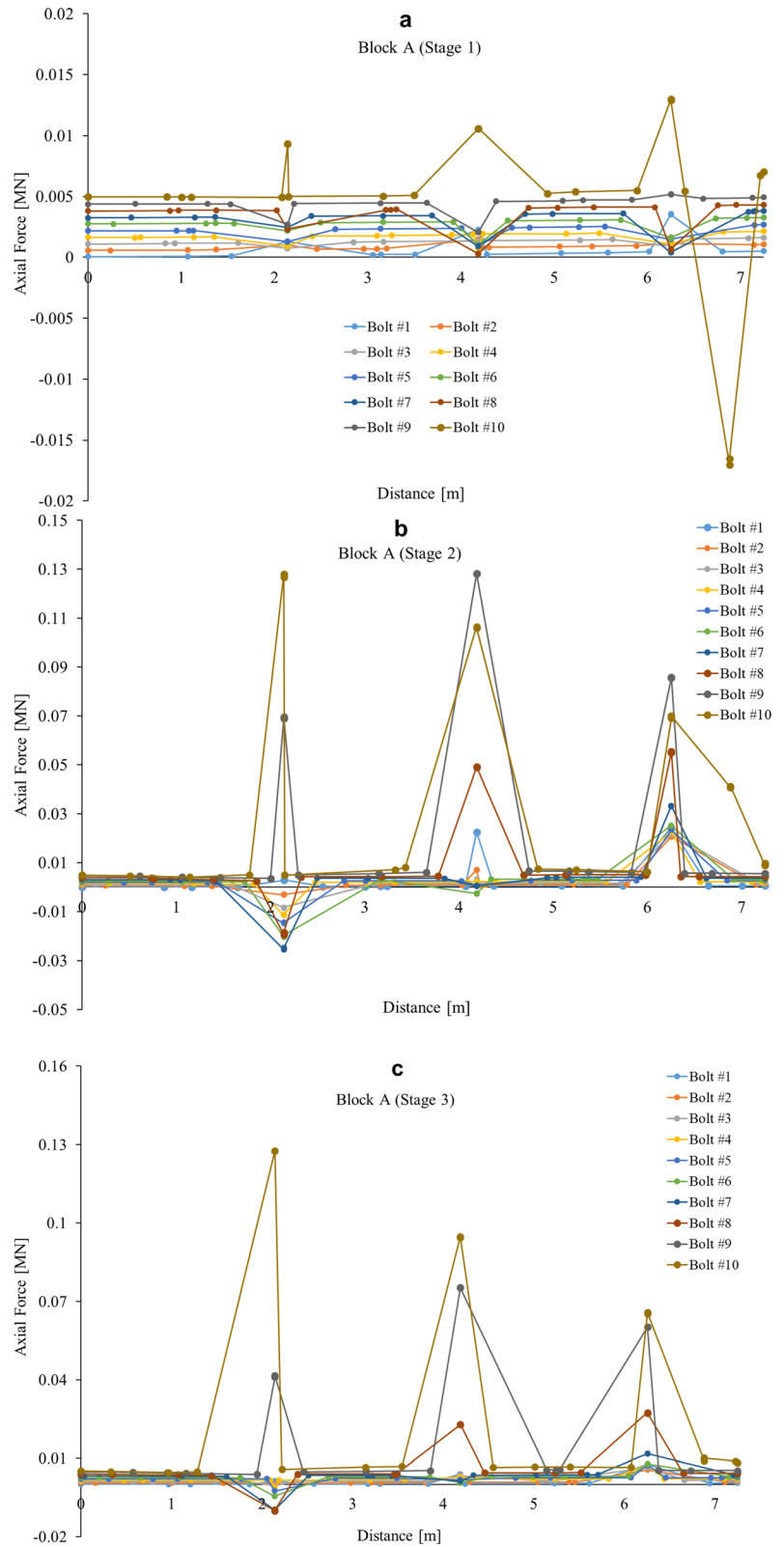
References

Adhikary DP, Dyskin AV, Jewell RJ (1997) A study of the mechanism of flexural toppling failure of rock slopes. Rock Mech Rock Eng 30(2):75–93

Alejano LR, Alonso E (2005) Application of the "shear and tensile strength reduction technique" to obtain factors of safety of toppling and footwall rock slopes. In: Impact of human activity on the geological environment—ISRM Eurock 2005, pp 7–13

Alejano LR, Carranza-Torres C, Giani GP, Arzua J (2015) Study of the stability against toppling of rock blocks with rounded edges based on analytical and experimental approaches. Eng Geol 195:172–184

Alejano LR, Gomez-Marquez I, Martinez-Alegria R (2010) Analysis of a complex toppling-circular slope failure. Eng Geol 114(1–2):93–104

Amini M, Ardestani A (2019) Stability analysis of the north-eastern slope of Daralou copper open pit mine against a secondary toppling failure. Eng Geol 249:89–101

Amini M, Ardestani A, Khosravi MH (2017) Stability analysis of slide-toe-toppling failure. Eng Geol 228:82–96

Amini M, Majdi A, Veshadi MA (2012) Stability analysis of rock slopes against block-flexure toppling failure. Rock Mech Rock Eng 45(4):519–532

Amini M, Sarfaraz H, Esmaeili K (2018) Stability analysis of slopes with a potential of slide-head-toppling failure. Int J Rock Mech Min Sci 112:108–121

Aydan O, Kawamoto T (1992) The stability of slopes and underground openings against flexural toppling and their stabilisation. Rock Mech Rock Eng 25(3):143–165

Aydar E, Schmitt AK, Çubukçu HE, Akın L, Ersoy O, Şen E, Duncan RA, Atıcı G (2012) Correlation of ignimbrites in the central Anatolian volcanic province using zircon and plagioclase ages and zircon compositions. J Volcanol Geotherm Res 213–214:83–97

Azarafza M, Akgün H, Ghazifard A, Asghari-Kaljahi E (2020) Key-block based analytical stability method for discontinuous rock slope subjected to toppling failure. Comput Geotech 124:103620

Babiker AFA, Smith CC, Gilbert M, Ashby JP (2014) Non-associative limit analysis of the toppling-sliding failure of rock slopes. Int J Rock Mech Min Sci 71:1–11

Barla G, Borri-Brunetto M, Devin P, Zaninetti A (1995) Validation of a distinct element model for toppling rock slopes. In: 8th ISRM Congress, pp 417–421

Barton N (1989) Cavern design for Hong Kong rocks. In: Malone AW, Whiteside PGD (eds) The Seminar Rock cavern-Hong Kong. The Institution of Mining and Metallurgy, pp 179–202

Barton NR, Choubey V (1977) The shear strength of rock joints in theory and practice. Rock Mech 10(1–2):1–54

Beekman PH (1966) The Pliocene and Quaternary volcanism in the Hasan Dag-Melendiz Dag region. Bull MTA 66:90–105

Binal A (1996) Investigation of the instability mechanisms observed in volcano-sedimentary rocks at Aksaray-Ihlara valley. MSc thesis, Hacettepe University, Ankara (**in Turkish**)

Bobet A, Fakhimi A, Johnson S, Morris J, Tonon F, Yeung MR (2009) Numerical models in discontinuous media: review of advances for rock mechanics applications. J Geotech Geoenviron Eng 135(11):1547–1561

Bowa VM, Xia Y, Kabwe E (2018) Analytical technique for stability analyses of rock slopes subjected to block toppling failure. Min Technol 127(4):219–229

Brideau MA, Stead D (2010) Controls on block toppling using a three-dimensional distinct element approach. Rock Mech Rock Eng 43(3):241–260

Cai M, Kaiser PK, Tasaka Y, Minami M (2007) Determination of residual strength parameters of jointed rock masses using the GSI system. Int J Rock Mech Min Sci 44(2):247–265

Calcaterra D, Parise M (2010) Weathering as a predisposing factor to slope movements: an introduction. Geol Soc Lond Eng Geol Spec Publ 23:1–4

Cruden DM (1989) Limits to common toppling. Can Geotech J 26(4):737–742

Dawson EM, Roth WH, Drescher A (1999) Slope stability analysis by strength reduction. Geotechnique 49(6):835–840

Doğan U, Koçyiğit A, Yılmaz E (2019) Geomorphological evolutionary history of the Melendiz River Valley, Cappadocia, Turkey. Mediterr Geosci Rev 1(2):203–222

Elmo D, Stead D (2010) An integrated numerical modelling–discrete fracture network approach applied to the characterisation of rock mass strength of naturally fractured pillars. Rock Mech Rock Eng 43(1):3–19

Erguler ZA (2009) Field-based experimental determination of the weathering rates of the Cappadocian tuffs. Eng Geol 105:186–199

Evans RS (1981) An analysis of secondary toppling rock failures-the stress redistribution method. Q J Eng Geol Lond 14:77–86

Goodman RE, Bray JW (1976) Toppling of rock slopes. In: Proceedings of Speciality Conference Rock Engineering for Foundations and Slopes, Boulder, Colorado, ASCE, 2

Griffiths DV, Lane PA (1999) Slope stability analysis by finite elements. Geotechnique 49(3):387–403

Haas CJ (1975) Shear resistance of rock bolts. In: 10th annual meeting of American Institute of mining, metallurgical and petroleum engineers. pp 32–40

Haghgouei H, Kargar A, Amini R, M. Esmaeili K. (2020) An analytical solution for analysis of toppling-slumping failure in rock slopes. Eng Geol 265:105396

Hammah RE, Yacoub TE, Corkum B, Curran JH (2005) The shear strength reduction method for the generalized Hoek–Brown criterion. In: 40th US symposium on rock mechanics, Anchorage, Alaska

Hammah RE, Yacoub TE, Corkum B, Wibowo F, Curran JH (2007) Analysis of blocky rock slopes with finite element shear strength reduction analysis. In: 1st Canada–U.S. rock mechanics symposium, Vancouver, Canada, pp 329–334

Hammah RE, Yacoub T, Corkum B, Curran JH (2008) The practical modelling of discontinuous rock masses with finite element analysis. In: 42nd US rock mechanics symposium, pp 56–63

Hammah RE, Yacoub T, Curran JH (2009) Variation of failure mechanisms of slopes in jointed rock masses with changing

scale. In: 3rd CANUS rock mechanics symposium (Paper No. 3956), Toronto

Hoek E (2008) Practical rock engineering. Evert Hoek Consulting Engineer Inc., Toronto

Hoek E, Bray JW (1991) Rock slope engineering. Elsevier Science Publishing, New York, p 358

Hoek E, Carranza-Torres C, Corkum B (2002) Hoek–Brown failure criterion—2002 edition. In: 1st North American rock mechanics symposium, Toronto, pp 267–273

Kaşmer Ö, Ulusay R, Geniş M (2013) Assessments on the stability of natural slopes prone to toe erosion and man-made historical semi-underground openings carved in soft tuffs at Zelve Open-Air Museum (Cappadocia, Turkey). Eng Geol 158:135–158

Lanaro F, Jing L, Stephansson O, Barla G (1997) DEM modelling of laboratory tests of block toppling. Int J Rock Mech Min Sci 34(3–4):173e1-173e15

Le Pennec JL, Bourdier JL, Froger A, Temel A, Camus G, Gourgaud A (1994) Neogene ignimbrites of Nevsehir Plateau (central Turkey): stratigraphy, distribution and source constraints. J Volcanol Geotherm Res 63:59–87

Liu CH, Jaksa MB, Meyers AG (2010) Toppling mechanisms of rock slopes considering stabilization from the underlying rock mass. Int J Rock Mech Min Sci 47(2):348–354

Majdi A, Amini M (2011) Analysis of geo-structural defects in flexural toppling failure. Int J Rock Mech Min Sci 48(2):175–186

Mas ID, Pierce ME, Darcel C, Reyes-Montes J, Potyondy DO, Paul YR, Cundall PA (2011) The synthetic rock mass approach for jointed rock mass modelling. Int J Rock Mech Min Sci 48(2):219–244

Mehranpour MH, Kulatilake PHSW, Xingen M, He M (2018) Development of new three-dimensional rock mass strength criteria. Rock Mech Rock Eng 51(11):3537–3561

Mohtarami E, Jafari A, Amini M (2014) Stability analysis of slopes against combined circular–toppling failure. Int J Rock Mech Min Sci 67:43–56

Muralha J (2003) Parameter variability in the toppling stability of rock blocks. In: Proceedings of the 10th conference of the international society for rock mechanic, Johannesburg, South Africa, pp 849–854

Nichol SL, Hungr O, Evans SG (2002) Large-scale brittle and ductile toppling of rock slopes. Can Geotech J 39(4):773–788

Official Gazette (1990) Ihlara Vadisi Özel Çevre Koruma Bölgesi, Bakanlar Kurulu Kararı, 22 October 1990, No. 90/1117 (in Turkish)

Pain A, Kanungo DP, Sarkar S (2014) Rock slope stability assessment using finite element-based modelling—examples from the Indian Himalayas. Geomech Geoeng Int J 9(3):215–230

Rocscience Inc (2019a) RS2 Version 9.0—finite element analysis for excavations and slopes. https://www.rocscience.com. Toronto, ON, Canada. Accessed 18 Nov 2019

Rocscience Inc (2019b) Dips Version 7.0—graphical and statistical analysis of orientation data. https://www.rocscience.com. Toronto, Ontario, Canada. Accessed 25 Nov 2019

Roosta RM, Sadaghiani MH, Pak A (2005) Strength reduction technique in stability analysis of jointed rock slopes. Int J Civ Eng 3(3–4):152–165

Roy D, Maheshwari P (2018) Probabilistic analysis of rock slopes against block toppling failure. Indian Geotech J 48(3):484–497

Sagaseta C, Sanchez JM, Canizal J (2001) A general analytical solution for the required anchor force in rock slopes with toppling failure. Int J Rock Mech Min Sci 38(3):421–435

Sarfaraz H (2020) Stability analysis of flexural toppling failure using the Sarma's method. Geotech Geol Eng 38(4):3667–3682

Sarfaraz H, Amini M (2020) Numerical modeling of rock slopes with a potential of block-flexural toppling failure. J Min Environ 11(1):247–259

Sarfaraz H, Amini M (2020) Numerical simulation of slide-toe-toppling failure using distinct element method and finite element method. Geotech Geol Eng 38(2):2199–2212

Sarfaraz H, Khosravi MH, Amini M (2019) Numerical analysis of slide-head-toppling failure. J Min Environ 10(4):1001–1011

Sari M (2009) The stochastic assessment of strength and deformability characteristics for a pyroclastic rock mass. Int J Rock Mech Min Sci 46(3):613–626

Sari M (2019) Stability analysis of cut slopes using empirical, kinematical, numerical and limit equilibrium methods: case of old Jeddah-Mecca road (Saudi Arabia). Environ Earth Sci 78(21):621

Sari M, Çömlekçiler F (2007) Kızılkaya ignimbiritlerinde görülen süreksizliklerin incelenmesi ve kaya kütlesinin tanımlanması. S.Ü. Müh-Mim Fak Derg 23(1–2), 207–216 (in Turkish)

Scavia C, Barla G, Bernaudo V (1990) Probabilistic stability analysis of block toppling failure in rock slopes. Int J Rock Mech Min Sci Geomech Abstr 27(6):465–478

Shen J, Karakus M (2014) Three-dimensional numerical analysis for rock slope stability using shear strength reduction method. Can Geotech J 51(2):164–172

Smith JV (2015) Self-stabilization of toppling and hillside creep in layered rocks. Eng Geol 196:139–149

Spreafico MC, Cervi F, Francioni M, Stead D, Borgatti L (2017) An investigation into the development of toppling at the edge of fractured rock plateaux using a numerical modelling approach. Geomorphology 288:83–98

Stead D, Eberhardt E, Coggan JS (2006) Developments in the characterization of complex rock slope deformation and failure using numerical modeling techniques. Eng Geol 83(3):217–235

Stillborg B (1994) Professional users' handbook for rock bolting, 2nd edn. Trans Tech Publication, Clausthal-Zellerfeld, p 164

Sun C, Chen C, Zheng Y, Xia K, Zhang W (2018) Topping failure analysis of anti-dip bedding rock slopes subjected to crest loads. Int J Geotech Geol Engnng 12(11):685–693

Taşpınar M (2015) Ihlara Vadisi (Aksaray) Boyunca Kaya Düşmelerinin Değerlendirilmesi, MSc Thesis, Aksaray Universitesi (**in Turkish**)

Tatone BSA, Grasselli G (2010) ROCKTOPPLE: a spreadsheet-based program for probabilistic block-toppling analysis. Comput Geosci 36(1):98–114

Topal T, Doyuran V (1997) Engineering geological properties and durability assessment of the Cappadocian tuff. Eng Geol 47(1–2):175–187

Ulusay R, Gokceoglu C, Topal T, Sonmez H, Tuncay E, Erguler ZA, Kasmer O (2006) Assessment of environmental and engineering geological problems for the possible re-use of an abandoned rock-hewn settlement in Urgüp (Cappadocia), Turkey. Environ Geol 50(4):473–494

Varnacı-Uzun F, Somuncu M (2015) Evaluation of the sustainability of tourism in Ihlara Valley and suggestions. Eur J Sustain Dev 4(2):165–174

Vlachopoulos N, Cruz D, Tatone BSA, Lisjak A, Mahabadi OK, Forbes B, Carrapatoso C (2020) The performance of axially loaded, fully grouted rock bolts based on pull-out experiments utilizing fiber optics technology and associated numerical modelling of such support elements. Geotech Geol Eng 38(2):1389–1407

Wyllie DC, Mah CW (2004) Rock slope engineering—civil and mining, 4th edn. Spon Press, New York

Yilmaz HM, Yakar M, Mutluoglu O, Kavurmaci MM, Yurt K (2012) Monitoring of soil erosion in Cappadocia region (Selime-Aksaray-Turkey). Environ Earth Sci 66(1):75–81

You G, Mandalawi MA, Soliman A, Dowling K, Dahlhaus P (2018) Finite element analysis of rock slope stability using shear strength reduction method. Soil Testing, Soil Stability and Ground Improvement, Sustainable Civil Infrastructures 1:227–235

Zanbak C (1983) Design charts for rock slopes susceptible to toppling. J Geotech Enginng 109(8):1039–1062

Zhang G, Wang F, Zhang H, Tang H, Li X, Zhong Y (2018) New stability calculation method for rock slopes subject to flexural toppling failure. Int J Rock Mech Min Sci 106:319–328

Zheng Y, Chen C, Liu T, Zhang H, Sun C (2019) Theoretical and numerical study on the block-flexure toppling failure of rock slopes. Eng Geol 263:105309